MAKING MOLECULAR MOVIE WITH MEV ELECTRONS*

X. Shen[†], X. Wang, SLAC National Accelerator Laboratory, Menlo Park, CA 94025, USA

Abstract

Ultrafast electron probes, complementary to x-ray free electron lasers, enable direct insight into structural dynamics in material, chemical, and biological sciences. SLAC National Accelerator Laboratory has constructed a mega-electron-volt (MeV) ultrafast electron diffraction (UED) system to serve ultrafast science experiments and instrumentation development. The system delivers high brightness electron beams of femtosecond pulse duration with outstanding machine stability performance, which enables visualization of ultrafast structural dynamics with atomic time and length scales, i.e., making molecular movies. In this paper, we review the performance of the SLAC MeV UED system, highlight recent results in material science and gas phase experiments, and give an outlook for future developments.

INTRODUCTION

Visualization of structural changes reveals the strong correlation between structure and functionality of matter. Electrons and x-rays with short wavelength ($\lesssim 1$ Å) and short pulse durations ($\lesssim 100$ fs) are the most viable probes for this challenging task with atomic length and time scales. While x-ray mainly interacts with atomic electrons, electrons are sensitive to both electrons and nuclei. Electrons have $10^4 - 10^6$ times larger scattering cross sections and less radiation damage per elastic scattering event [1]. Electrons are charged particles such that they can be easily manipulated by accelerating structures and electro-magnetic lenses in a compact setup. The good properties of electrons have driven development of ultrafast electron diffraction and microscopes (UED and UEM) in the last few decades [2-10].

So far, most UED systems are operating with kilo-electron-volt (keV) DC electron sources. However, due to the strong space-charge forces at such low electron energies, the electron bunches undergo substantial length expansion as it propagates [11]. Therefore, it becomes practically impossible to produce a keV electron bunch with ∼ 100 fs pulse duration at the specimen with more than a few hundred electrons [12]. Even with high efficiency single-electron detectors, obtaining a high signal-to-noise ratio diffraction pattern, which generally requires at least 10^6 electrons at the sample, is very difficult in the sense of apparatus stability, sample exposure time, sample heat load deposited by pump pulse, etc.

The temporal resolution barrier due to strong space-charge forces can be overcome by implementing an rf

photoinjector as high brightness electron sources [13, 14]. The accelerating field of a rf photoinjector normally exceeds 100 MV/m, which is much higher than the 10-20 MV/m level for the dc photocathode. Electrons extracted in a rf photoinjector are rapidly accelerated to mega-electron-volt (MeV) level, such that the space-charge forces are greatly suppressed. It then becomes possible to group into a bunch of ∼ 100 fs duration with up to three orders of magnitude more electrons. Moreover, the relativistic nature of the MeV electron probe naturally solves the problem of velocity mismatch between the pump pulse and probe beam which is critical when it comes to gas phase samples [15]. The more energetic electrons also come with a larger penetration depth, which enables implementation of thicker specimens.
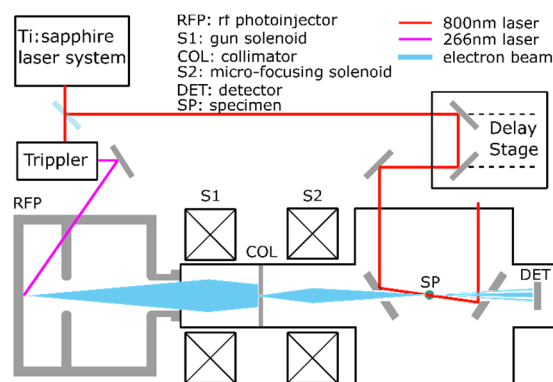
Figure 1: A schematic diagram of the SLAC MeV UED system.

SLAC MEV UED SYSTEM

SLAC recently launched a UED/UEM Initiative [16] aiming at developing the world's leading ultrafast electron scattering instruments. The first stage of the Initiative was to construct an MeV UED system. Figure 1 shows a schematic diagram for the SLAC MeV UED system. A Ti:sapphire laser system produces a 5 mJ 800 nm laser pulse which is split into two parts: a pulse goes to the pump line, while the other pulse is frequency tripled to 266 nm UV laser pulse to illuminate the photocathode at a 70° angle of incidence to generate femtosecond electron bunches. The 80 MV/m accelerating gradient in the rf photocathode rapidly accelerates electron bunches to 3.7 MeV, where the effect of space-charge forces is strongly reduced. The gun solenoid (S1) right after the rf photocathode is used to adjust the beam divergence at the exit of the rf photocathode, which effectively adjusts the beam size on the retractable collimator (COL) located at 0.4m downstream of the gun solenoid. The four pin holes on the collimator, with diameter of 100 um, 200 um, 500 um, and 1000 um, respectively, can be flexibly in-

serted to select the central part of the beam with corresponding pinhole size, which effectively filters beam emittance. The emittance-filtered beam can be easily focused into small probe size at the specimen (SP) in the sample chamber by the micro-focusing solenoid (S2) located at 0.45m downstream of the collimator. The pump pulse illuminates the front surface of the specimen with an incidence angle of 50 mrad. The diffraction pattern is capture by a detector system (DET) equipped with an Andor iXon Ultra 888 electron multiplying charge-coupled device (EMCCD) camera [17].

The SLAC MeV UED system operates at 180 Hz repetition rate with outstanding machine stabilities. The typical values for the rf amplitude and phase stability of the gun field are 2×10^{-4} rms and 25 fs rms over hours, while the typical in-loop timing error between the laser and the low-level rf is 29 fs rms. The normalized emittance of the electron beams was measured to be better than 20 nm-rad. The instrumental temporal resolution was demonstrated to be 100 fs rms [18].

HIGHLIGHT OF RECENT SCIENCE RESULTS AT SLAC MEV UED SYSTEM

The unique probe-beam capability and outstanding machine stability of the SLAC MeV UED system has facilitate many ultrafast dynamics studies in material science [19-22] and gas-phase experiments [23-25]. In the following, selected experiment results are reviewed.

Dynamic structural deformations of monolayer MoS$_2$ [19]

The unique optical and electronic properties of two-dimensional materials are intrinsically coupled to struc-

tural properties with strain and interfacial coupling acting as a means to engineer and modulate these responses. To gain insight understanding of these processes, direct observation of the dynamical structural response of monolayer MoS$_2$ under femtosecond laser excitation was carried out in the SLAC MeV UED system. Figure 2a shows a schematic of the experimental setup. Large-area, single-crystal monolayer MoS$_2$ was pumped by 400 nm laser pulse and probed by 3.7 MeV electrons. By varying the delay between the pump-laser and the probe-electron, the laser-excited dynamical structural response was captured from the diffraction patterns. Figure 2b shows temporal evolution of the intensities $\Delta I/I$ of two lowest-order diffraction peaks. The inset shows an overlay of the measured long-recovery dynamics (red solid) with simulation results (blue dashed). These results show reversible large in-plane atomic displacement. Figure 2c shows Time-dependent shifts $\Delta Q/Q$ and broadening $\Delta\sigma/\sigma$ for the $\{11\bar{2}0\}$ reflection showing concurrent strains and broadening associated with rippling of the monolayer developing on few picosecond time-scales. These observations reveal that the MoS$_2$ film can sustain giant strains and intense photoexcitation conditions in a reversible fashion. This indicates new possibilities for all-optical dynamic control of wrinkling degrees of freedom and their coupled electronic and optical responses. For example, the peak strains extracted above correspond to spatially inhomogeneous modulations in the band gap of ~0.1 eV and present novel opportunities for tuning the band structure with light on picosecond time-scales. In this experiment, the atomic scale temporal resolution and the high reciprocal-space resolution of the SLAC MeV UED system enabled successful capture of the ultrafast strain and wrinkling dynamics.
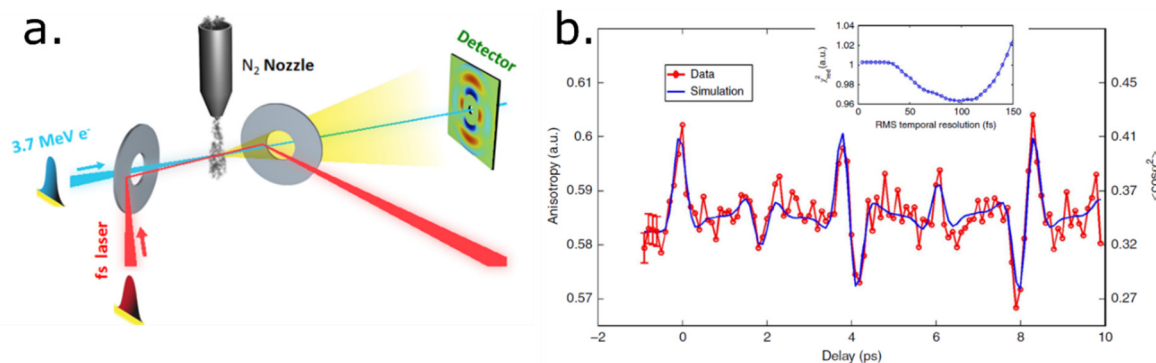
Figure 3: (a) Schematic of experimental setup for N$_2$ experiment. A 3.7-MeV pulsed electron beam (blue) is directed towards a nitrogen gas jet (grey). The gas jet is introduced into the vacuum chamber using a pulsed nozzle (black). The pump laser pulse (red) is deflected by two ring-shaped mirrors. The laser propagates at a small angle (~5°) with respect to the electron beam as it traverses the target, and is then deflected away from the detector by the second mirror. The electron diffraction pattern is recorded with a phosphor screen located 3.1m downstream from the interaction region. The unscattered electron beam is transmitted through a hole in the phosphor screen. (b) Anisotropy in the diffraction patterns from experimental data (red) and simulation (blue) versus time. Statistical error bars for the first few points (before alignment) are shown to illustrate the uncertainty of this measurement. The right-hand side axis gives the degree of alignment $< cos^2 \alpha >$ for the simulated curve. Reduced χ^2 error versus RMS temporal resolution in the four-parameter fit is shown in the inset, with a best fit of 100 fs rms temporal resolution (from [23]).
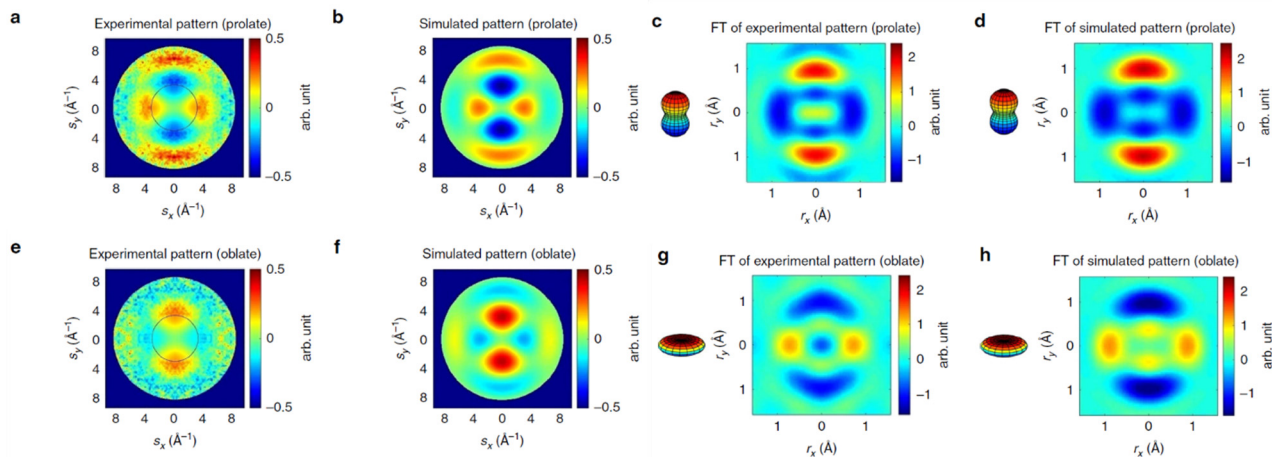
Figure 4: (a) Experimentally measured and (b) simulated diffraction-difference patterns of the prolate distribution. Images shown in c,d are Fourier transforms of a,b, respectively. The Fourier transform of the diffraction-difference patterns show the changes in the angular distribution of the molecules. The positive regions (red color) indicate where the population has increased and the negative regions (blue color) indicate where the population has decreased. (e) Experimentally measured and (f) simulated diffraction-difference pattern of the oblate distribution. Images shown in g,h are Fourier transforms of e,f, respectively. In patterns (a,e), the data inside the black circles are missing due to the beam stop. They are obtained by extrapolating the pattern and letting the counts smoothly go to zero towards the center. For illustrative purpose, angular distributions are shown on the side of panel (c,d,g,h) for visual guidance. In these angular distributions, the color code indicates polar angle (from [23]).

Rotational dynamics in laser aligned N_2 [23]

Gaseous molecules are ideal to study prototypical processes in chemistry. Characterization of how the individual nuclei of a molecule move relative to one another in a molecular transformation is crucial to understand chemical reactivity. With instrumental resolutions at atomic length and time scales, the SLAC MeV UED system has demonstrated its unique capability for this challenging task by a N_2 laser alignment experiment. Figure 3a shows a schematic of the experiment set up. The 3.7 MeV electron pulse (blue) is diffracted from the nitrogen gas jet (grey), which is introduced into the vacuum chamber by a pulsed nozzle (black). The diffraction pattern is captured by a phosphor screen and a detector. The 800-nm alignment laser pulse (red) is directed to the target and removed from the vacuum chamber by two holey mirrors at a 45° angle to the electron beam. The alignment laser pulse induces a dipole along the N_2 molecular axis. The interaction of the induced dipole with the electric field forces the N_2 molecules oscillate about the electric field polarization. The initially isotropic ensemble of N_2 molecules becomes anisotropic. The prolate (most molecules aligned with electric field polarization) and oblate (most molecules aligned perpendicular to electric field polarization) distributions occur periodically. The degree of alignment is characterized by the factor $< \cos^2 \alpha >$, where α is the polar angle between molecular axis and the electric field polarization. For an isotropic distribution $< \cos^2 \alpha >= 1/3$. On the other hand, the degree of alignment can also be deduced from diffraction-difference pattern, which is the difference between a diffraction pattern and a reference diffraction pattern with isotropic distribution. For prolate distribution, the diffraction-difference pattern is highly anisotropic with its intensities localized in a certain area, while for oblate distribution, the intensities are localized in another area which is perpendicular to the one for the prolate distribution. The ratio between total intensities in these two areas, which is called anisotropy, gives an estimation of degree of alignment. Figure 3b shows temporal evolution of measured (red) and simulated (blue) anisotropy, as well as corresponding $< \cos^2 \alpha >$. The two are in good agreement. The inset shows the reduced χ^2 error versus rms temporal resolution for the simulation. The best fit gives 100 fs rms temporal resolution. Figure 4a and 4b shows experimental and simulated diffraction-difference patterns for the prolate distribution. As discussed before, the diffraction patterns are highly anisotropic. Figure 4c and 4d shows the Fourier transforms of the diffraction-difference patterns in Fig. 4a and 4b, respectively. These Fourier transformed images display the autocorrelation of the molecular structure convoluted with angular distribution and projected onto the detector plane. For a diatomic molecule like N_2, the autocorrelation is directly related to the molecular image. In Fig. 4c and 4d, the positive regions indicate more N_2 molecules are localized parallel to the laser polarization, while the negative regions show less N_2 molecules population. Similarly, Fig. 4e and 4f show the diffraction-difference pattern for an oblate distribution, while Fig. 4g and 4h show corresponding Fourier transforms. In this case, the N_2 molecules are aligned perpendicular to the laser polarization. In summary, thanks to the 0.76 Å spatial resolution and 100 fs rms temporal resolu-

tion provided by the SLAC MeV UED system, molecular movie from N_2 laser alignment is successfully captured.

CONCLUSIONS

A SLAC MeV UED system with resolutions at atomic length and time scales has been constructed and commissioned to serve ultrafast dynamics studies in material and chemical sciences. Continuous efforts have been devoted to the development of next generation ultrafast electron scattering instruments. A strong lens has been installed to reduce the probe size to a few μm and eventually to sub-μm. This will greatly ease the technical challenge in sample preparation for UED. This also enables study over single crystalline domains. A cryo sample stage has been installed such that sample temperature can be lowered to 34 K. This provides great opportunities for studies such as phase transitions of strongly correlated systems. A direct electron detector is under commissioned to explore higher spatial resolution and enable features of single electron counting and single-shot image acquisition. An rf bunching cavity will be installed to compress the pulse duration to 10-fs level with order-of-magnitude more charge. Combined with new time-of-arrival and time stamping technique, it is possible to reach 20-fs temporal resolution. The idea combining THz and x-ray pump with MeV electron probes will open new opportunities for groundbreaking science studies.

REFERENCES

[1] R. Henderson, *et al.*, *Biophys.,* vol. 28, p. 171, 1995.

[2] W. E. King, *et al.*, *Appl. Phys.,* vol. 97, p. 111101, 2005.

[3] A. H. Zewail, Annu. *Rev. Phys. Chem.,* vol. 57, p. 65, 2006.

[4] G. Sciaini and R. J. D. Miller, *Rep. Prog. Phys.*, vol. 74, p. 096101, 2011.

[5] P. Musumeci and R. K. Li, in *ICFA Beam Dynamics Newsletter* No. 59, edited by J. M. Byrd and W. Chou (International Committee for Future Accelerators, pp. 13–33, 2012.

[6] B.W. Reed, *et al.*, *Microsc. Microanal.*, vol. 15, p. 272, 2009.

[7] A. H. Zewail, *Science,* vol. 328, p. 187, 2010.

[8] A. H. Zewail and J. M. Thomas, *4D Electron Microscopy: Imaging in Space and Time*, Imperial College Press, London, 2010.

[9] N. D. Browning, *et al.*, *Handbook of Nanoscopy*, Wiley-VCH Verlag GmbH & Co. KGaA, 2012.

[10] D. J. Flannigan and A. H. Zewail, *Acc. Chem. Res.,* vol. 45, p. 1828, 2012.

[11] B. J. Siwick, *et al.*, *J. Appl. Phys.*, vol. 92, p. 1643, 2002.

[12] X. Wang, *et al.*, *Rev. Sci. Instrum.*, vol. 80, p. 013902, 2009.

[13] X. J. Wang, *et al.*, in *Proceedings of 2003 Particle Accelerator Conference*, IEEE, Portland, OR, USA, pp. 420, 2003.

[14] X. J. Wang, *et al.*, *J. Korean Phys. Soc.*, vol. 48, p. 390, 2006.

[15] J. C. Williamson and A. H. Zewail, *Chem. Phys. Lett.*, vol. 209, p. 10, 1993.

[16] SLAC Strategic Plan, 2014, *https://www6.slac.stanford.edu/files/Strategic_Plan_2014.pdf*

[17] See *http://www.andor.com/* for information about Andor iXon Ultra 888 EMCCD.

[18] S. P. Weathersby, *et al.*, "Mega-electron-volt ultrafast electron diffraction at SLAC National Accelerator Laboratory", *Rev. Sci. Instrum.*, vol. 86, p. 073702, 2015.

[19] E. M. Mannebach, *et al*., "Dynamic Structural Response and Deformations of Monolayer MoS_2 Visualized by Femtosecond Electron Diffraction", *Nano Lett.*, vol. 15, p. 6889, 2015.

[20] K. Sokolowski-Tinten, *et al*., "Thickness-dependent electron–lattice equilibration in laser-excited thin bismuth films", *New Journal of Physics,* vol. 17, 2015.

[21] T. Chase, *et al.*, "Ultrafast electron diffraction from non-equilibrium phonons in femtosecond laser heated Au films", *Appl. Phys. Lett.,* vol.108, p. 041909, 2016.

[22] A. H. Reid, *et al*., "Ultrafast spin-lattice coupling in laser-excited FePt nanoparticles", submitted to *Physical Review Letters*.

[23] J. Yang, *et al.*, "Diffractive imaging of a rotational wave-packet in nitrogen molecules with femtosecond megaelectronvolt electron pulses", *Nature Communications* vol. 7 , 2016.

[24] J. Yang, *et al.*, "Diffractive Imaging of Coherent Nuclear Motion in Isolated Molecules", accepted by *Physical Review Letters*.

[25] J. Yang, *et al.*, "Femtosecond Gas Phase Electron Diffraction with MeV Electrons", *Faraday Discuss.* vol. 87, 2016.